JACS
JOURNAL OF THE AMERICAN CHEMICAL SOCIETY

Article

pubs.acs.org/JACS

Physico-chemical Control over the Single- or Double-Wall Structure of Aluminogermanate Imogolite-like Nanotubes

Antoine Thill,*[,†,⊥] Perrine Maillet,[†] Béatrice Guiose,[†] Olivier Spalla,[†,⊥] Luc Belloni,[†] Perrine Chaurand,[‡,⊥] Mélanie Auffan,[∥,⊥] Luca Olivi,[§] and Jérôme Rose[∥,⊥]

[†]CEA Saclay, IRAMIS, Laboratoire Interdisciplinaire sur l'Organisation Nanométrique et Supramoléculaire, 91191 Gif-sur-Yvette cedex, France

[‡]Aix-Marseille University, CEREGE, UMR 6635, 13545 Aix-en-Provence cedex 4, France

[§]ELETTRA, Synchrotron Light Source, 34012 Trieste, Italy

[∥]CNRS, CEREGE, UMR 6635, 13545 Aix-en-Provence cedex 4, France

[⊥]International Consortium for the Environmental Implications of Nanotechnology, iCEINT, http://www.i-ceint.org, France

Supporting Information

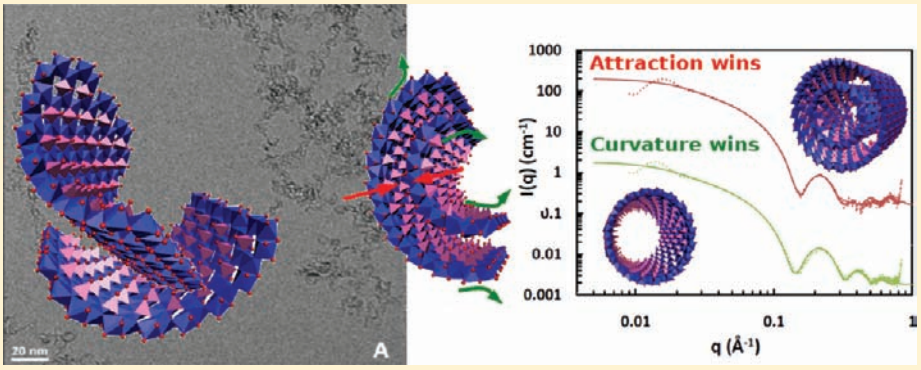

ABSTRACT: It is known that silicon can be successfully replaced by germanium atoms in the synthesis of imogolite nanotubes, leading to shorter and larger AlGe nanotubes. Beside the change in morphology, two characteristics of the AlGe nanotube synthesis were recently discovered. AlGe imogolite nanotubes can be synthesized at much higher concentrations than AlSi imogolite. AlGe imogolite exists in the form of both single-walled (SW) and double-walled (DW) nanotubes, whereas DW AlSi imogolites have never been observed. In this article, we give details on the physicochemical control over the SW or DW AlGe imogolite structure. For some conditions, an almost 100% yield of SW or DW nanotubes is demonstrated. We propose a model for the formation of SW or DW AlGe imogolite, which also explains why DW AlSi imogolites or higher wall numbers for AlGe imogolite are not likely to be formed.

INTRODUCTION

Achieving perfect control over the morphology of nanoparticles is the everyday job of many researchers around the world. This goal is essentially motivated by the fact that the different morphologies strongly influence the properties of the final products such as for carbon nanotubes or quantum dots. Among the vast family of available nanoparticles, imogolite is a clay nanotube for which perfect control of the diameter is possible. Imogolites were first observed in volcanic soils.[1] They are natural aluminosilicate nanotubes having the general formula $(OH)_3Al_2O_3SiOH$ with a 2 nm external diameter and up to micrometers in length. The local structure of imogolite has been proposed by Cradwick et al. in 1972,[2] and since then it has been widely characterized using multiscale approaches like X-ray diffraction (XRD),[3] solid-state nuclear magnetic resonance (NMR),[4,5] infrared spectroscopy (IR),[6] and transmission electron microscopy (TEM).[2,3,7] The local structure proposed by Cradwick et al. consists of a Gibbsite sheet curved by the adsorption of orthosilicate tetrahedra into the vacancies of the aluminum dioctaedral layer. Control of the imogolite diameter has been achieved by replacing silicon with germanium atoms.[8] The difference in nanotube diameter is explained by the local structure of the imogolite. Indeed, the adsorption of the SiO_4 or GeO_4 tetrahedra is responsible for the curvature of the Gibbsite layer, the Si−O and Ge−O bonds of the tetrahedra being stretched when covalently linked by three Si−O−Al or Ge−O−Al bonds in the dioctahedral layer. This size mismatch is responsible for the creation of a spontaneous curvature of the Gibbsite layer.[9] This has been confirmed recently by Konduri et al. both for AlSi imogolite and for AlGe imogolite using molecular modeling.[10,11] Their

Received: October 17, 2011
Published: January 31, 2012

   dx.doi.org/10.1021/ja209756j | J. Am. Chem. Soc. 2012, 134, 3780−3786

model is able to explain the difference in diameter between pure Si imogolite and pure Ge imogolite. Other modeling approaches were applied for the case of AlSi imogolites.[12−14] They confirm the role of Al−O and Si−O bond stretching but also point out the importance of the hydrogen-bond network close to the inner and outer walls of the imogolite nanotube.

The impressive monodispersity in imogolite nanotube diameter has motivated research on their formation mechanism. Synthesis protocols to produce imogolite were quickly developed. Farmer et al. were the first to obtain synthetic imogolite using low concentrations of $AlCl_3$ and SiO_2 monomers as starting materials (millimolar concentrations of the reagents).[9] It has been discovered recently that the AlGe imogolite analogues can be obtained in large amount (initial decimolar concentrations of the reagents) with a formation kinetic comparable to the aluminosilicate imogolite obtained from millimolar concentrations of the reagents.[15] At 95 °C, 5 days are necessary to grow the aluminogermanate nanotubes from a concentrated suspension of protoimogolites. It was known from IR and Raman spectroscopy that the proto-imogolites have the same local structure as the final nanotubes.[16] Using SAXS experiments after hydrolysis of the germanium and aluminum precursors and before sample heating treatments, Levard et al. demonstrated that the Ge protoimogolite most probably consists of roof-tile shaped nanotube pieces.[17] A detailed analysis of the very early stage of the protoimogolite formation mechanism was also performed recently by Yucelen et al.[18] for the AlSi imogolites using nuclear magnetic resonance and electrospray ionization mass spectroscopy. In the work of Levard et al., only an average structure of the protoimogolite was proposed. According to Yucelen et al., protoimogolite suspensions contain a mixture of many different structures. However, the initial conclusion regarding intermediate curved species having the same local structure as the final imogolite nanotubes and a natural curvature of the same type is largely confirmed. In the case of AlGe imogolites, Maillet et al. showed that after a 5 days heating period, protoimogolites not only form single-walled (SW) nanotubes as for the natural AlSi imogolite but also double-walled (DW) nanotubes.[19] The diameter of the DW nanotubes (4 nm) is slightly larger than that of the SW nanotubes (3.5 nm). Maillet et al. also showed that these roof-tile shaped protoimogolites transform at a constant volume fraction into both SW or DW nanotubes that grow essentially through a tip−tip collision mechanism.[20] The DW nanotubes grow at lower rate due to a decrease of the tip−tip linkage probability.

In the original paper that showed the existence of SW and DW nanotubes, the two forms were obtained using a variation of the total reactant concentration.[19] At an initial concentration of 0.25 M (mol L^{-1}) of aluminum perchlorate, DW nanotubes are obtained, whereas at 0.5 M initial concentration of aluminum perchlorate, SW nanotubes are obtained. The conditions allowing this unexpected DW structure to form were not understood. The objective of this article is to explore the physicochemical conditions controlling the production of nanotubes having the SW, DW, or a mixture of both SW/DW structures. The possibility of forming multi wall AlGe imogolite-type structures or DW AlSi imogolite is also discussed.

EXPERIMENTAL SECTION

Synthesis of the Aluminogermanate Nanotubes. Tetraethoxygermanium is added to an aluminum perchlorate solution until an Al/Ge ratio of 2 is obtained. The initial aluminum perchlorate concentrations C are varied between 0.25 and 0.75 M. The mixture is then slowly hydrolyzed by addition of a NaOH solution having the same concentration as the aluminum perchlorate solution to reach a hydrolysis ratio (OH/Al) of 2. In some experiments, the hydrolysis ratio was varied from 0.5 to 3.0 using a 1 M NaOH solution. The obtained solution is stirred overnight and then introduced into an oven at 90 °C for 5 days. After the 5 days of growth, the samples are removed from the oven and stored at ambient temperature until analysis.

To observe the transition from SW to DW nanotube structures, two types of experiments have been performed. First, the total concentration of reactant has been changed from 0.25 to 0.75 M. It has been previously observed that at low concentration, DW imogolite nanotubes tend to form, whereas at large concentration, SW nanotubes are obtained. The second type of experiments consists of changing the hydrolysis ratio R = OH/Al at a constant reactants concentration. Starting from an aluminum perchlorate suspension at a concentration of 0.5 M, a 1 M sodium hydroxide solution is slowly introduced in different samples to reach a hydrolysis ratio R of 0.25, 0.5, 1, 1.5, 2, 2.5, 2.75, and 3. The samples with the different values of the hydrolysis ratio are then aged at 90 °C in an oven for 5 days.

Infrared Spectroscopy. Infrared spectra were recorded using a Bruker Vertex 70 FTIR spectrometer with a resolution of 4 cm^{-1} at room temperature. About 1 mg of dried sample was mixed with 100 mg of potassium bromide powder and then pressed into a transparent disk. IR spectra were collected by averaging 20 scans in the range 4000−400 cm^{-1}.

Small-Angle X-ray Scattering. The experimental setup for small-angle X-ray scattering experiments includes a rotating anode and collimating optics providing a monochromatic beam (λ = 0.1548 nm) of 2 × 2 mm^2 at the sample position with a total incident flux of 8 × 10^7 photons/s. The transmitted flux is measured continuously with a photodiode placed on the beam stop. A MAR research X-ray sensitive 300 mm plate detector is placed after the output window of the vacuum chamber at a distance of 1200 mm from the sample. A ratio q_{max}/q_{min} of 34 is reached with q_{max} = 0.5 $Å^{-1}$ and q_{min} = 0.015 $Å^{-1}$. The scattering vector q is defined as $q = k_d - k_i$ (the wave vectors of the incident and scattered beams) and has a modulus of $q = 4\pi/\lambda \sin(\theta)$, where λ is the incident wavelength and 2θ is the scattering angle. The samples are introduced in kapton cells. The counting time is 3600 s, and the signal is corrected for background. Standard procedures are applied to obtain the scattered intensity in cm^{-1} as a function of scattering vector q.[21]

Cryo-TEM. Cryo-TEM observations of the samples were performed on a JEOL 2100F electron microscope using an accelerating voltage of 200 kV. We have operated the cryo-TEM microscope using the minimum dose system. In this mode, a maximum electron flux of 10 electrons per $Å^2$ per second is applied on the sample. The solutions were quickly frozen in liquid ethane and observed at a temperature of −180 °C in slight underfocus conditions (100−200 nm). So, it has been possible to collect contrasted images up to a magnification of 200 000 without significant sample structure modifications. Three successive image acquisitions were necessary to observe significant beam damage.[19]

EXAFS. Extended X-ray absorption fine structure spectroscopy (EXAFS) spectra were recorded in transmission mode on beamline 11.1 at the ELETTRA synchrotron (Trieste, Italy). Spectra were acquired using a Si(111) monochromator above the Ge K-edge (11 103 eV). The ion chambers for incident and transmitted beam were filled with Ar and N_2. The high signal/noise ratio permitted one to scan EXAFS spectra up to 16 $Å^{-1}$. EXAFS spectra were analyzed using standard procedures for data reduction with a set of software developed by Michalowicz.[22,23] EXAFS oscillations were theoretically recalculated using amplitude and phase functions obtained with the FEFF8 code.[24] FEFF functions were validated for each scattering path by modeling the spectra of well-characterized crystalline model compounds of GeO_2 and Ge-talc synthesized by the group of F. Martin.[25]

dx.doi.org/10.1021/ja209756j | J. Am. Chem. Soc. 2012, 134, 3780−3786

RESULTS AND DISCUSSION

SW/DW Structural Control through R = OH/Al variations. We have first explored the effect of the hydrolysis ratio on the SW or DW structure of the imogolite.

The effect of this parameter on the control of the nanotube morphology is not yet known. In Figure 1A, the signal is

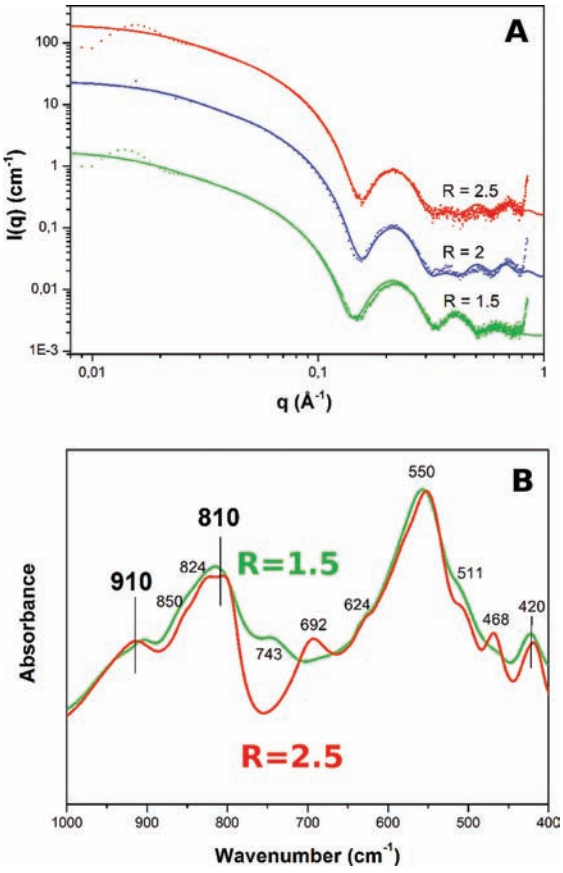

Figure 1. (A) SAXS measurements obtained for samples with an initial aluminum perchlorate concentration of 0.5 M and hydrolysis ratios R = 1.5, 2, and 2.5. For clarity, the signal of the R = 1.5 sample has been divided by 10 and the signal of the R = 2.5 sample has been multiplied by 10. The continuous lines correspond to the scattering form factor of model SW or DW tubes (see the Supporting Information). (B) IR spectra for the hydrolysis ratios R = 1.5 and R = 2.5.

unambiguously confirming the presence of imogolite nanotubes at R between 1.5 and 2.5. When taking into account the variable dilution due to the modification of the hydrolysis ratio, the final aluminum concentrations are 0.28, 0.25, and 0.22 M for R = 1.5, 2, and 2.5, respectively. The shapes of the oscillations at large angles are very different for the imogolite nanotubes obtained at R = 1.5 and at R = 2 and 2.5. At R = 1.5, the regular oscillations correspond to a single-walled (SW) imogolite nanotube, whereas at R = 2 and 2.5, the irregular oscillations are the signature of a double-walled (DW) structure.[19] To confirm the SW and DW morphologies and to quantify the radius of the nanotubes, the SAXS curves obtained at R = 1.5, 2, and 2.5 were compared to imogolites nanotube scattering models. For the SW nanotubes, the SAXS curve is modeled by an open cylinder structure with an external radius of 1.9 nm, a wall thickness of 6 Å, and an average scattering length density of 2.65×10^{11} cm^{-2}. In the case of DW imogolite nanotubes, the same wall thickness and average scattering length density are used. The external radius of the internal tube is 1.3 nm, and the external radius of the external tube is 2.15 nm.

Figure 1B shows the IR spectra of aluminogermanate imogolite-like nanotubes with SW (R = 1.5) and DW (R = 2.5) morphology in the range 400−1000 cm^{-1}. The spectra of the two samples are very similar, which is in agreement with the assumption that the local structures of SW and DW nanotubes are identical. First, the characteristic stretching vibrations of Ge−O, in AlGe imogolite nanotubes at 910 and 810 cm^{-1}, are found in accordance with previous works.[8,15,26] Between these two characteristic bands, Wada et al. have assigned the 830−850 bands to OH vibrations thanks to the study of the effect of deuteration on the IR spectra of synthetic Ge and Si imogolites. Finally, the bands at 550 and 420 cm^{-1} have been ascribed by the same authors to the stretching vibrations of Al−O.[8] However, it should be pointed out that small differences exist between the SW and DW structure IR spectra. In particular, in the DW structure, the two absorption bands at 468 and 692 cm^{-1} are not visible in the case of the SW structure. If we refer again to Wada et al.,[8] we can notice that their spectra also show two bands at 465 and 685 cm^{-1}, which they assigned to the Al−O stretching vibrations. In the SW structure, a new absorption band is observed at 743 cm^{-1}. In that case, the band probably corresponds to a shift of the 692 cm^{-1} band of the DW structure.

To summarize, IR spectroscopy has succeeded in distinguishing SW and DW structures. As this technique is widely used to characterize natural and synthetic imogolites, it can also be useful to predict their DW or SW morphologies. For instance, it is interesting to note that the DW spectrum of the aluminogermanate is very similar to those obtained by other authors,[8,15,16] indicating that the previously synthesized Ge-imogolites were probably DW nanotubes.

For the samples obtained at an hydrolysis ratio of less than 1.5 or more than 2.5, the SAXS signals did reveal the presence of nanostructured solids in suspensions, but none of the samples corresponds to an almost pure nanotube phase like for R between 1.5 and 2.5. It is difficult to extract directly from the SAXS curves a well-defined structure for these samples. It is possible that at low values of R protoimogolites are already obtained. A protoimogolite solution is most probably a mixture of roof-tile shaped imogolite nanotube pieces.[17,18] Interestingly, the shapes of the SAXS curves obtained at R = 0.25, 0.5, and 1 are very similar. It seems that in the first stage of the hydrolysis ratio increase, similar objects are formed.

Figure 2 shows the obtained cryo-TEM image for R = 2, C = 0.5 M before the heat treatment. Nanoparticles of roughly 5−10 nm are clearly observed. They present a curved shape and are aggregated. No evidence of the presence of nanotubes is obtained at this stage of the reaction. The roof-tile shape of the protoimogolite nanoparticles is strongly confirmed by these images. Besides the shape information, cryo-TEM reveals that the protoimogolite pieces tend to stack and form aggregates.

SW/DW Structural Control through Modification of the Concentration. The second route available for the control of the final nanotube structure consists of modifying the reactant concentration. We have varied the initial aluminum concentration from 0.25 to 0.75 M, keeping the stoichiometric ratio (Al/Ge = 2, OH/Al = 2). Figure 3 shows the scattering curves obtained for the samples after 5 days of growth at 90 °C. The oscillations at large q are characteristic of the SW or DW structures. They change progressively from a typical DW signal at low concentration to a typical SW signal at large

dx.doi.org/10.1021/ja209756j | J. Am. Chem. Soc. 2012, 134, 3780−3786

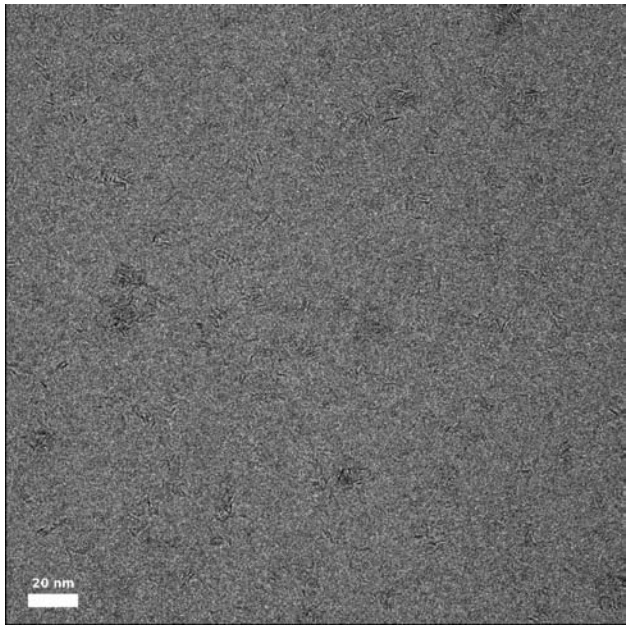

Figure 2. Cryo-TEM image of the solid phase obtained for an initial aluminum perchlorate concentration of 0.5 M and a hydrolysis ratio of 2 before the heat treatment.

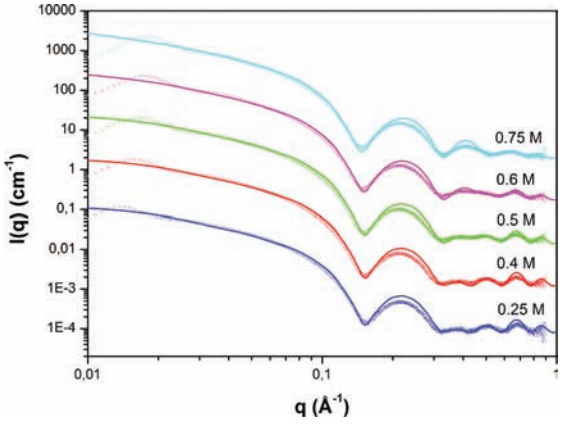

Figure 3. Scattering curves obtained after 5 days of growth at 90 °C starting from initial aluminum concentrations of 0.25, 0.4, 0.5, 0.6, and 0.75 M. The continuous lines are fits using a mixture of SW and DW in proportions given in Table 1. For clarity, the SAXS curves are shifted by a factor 0.01, 0.1, 1, 10, and 100 for 0.25, 0.4, 0.5, 0.6, and 0.75 M, respectively.

concentration. The transformation from one nanotube type to the other is not an abrupt transition, but the SW/DW proportion varies progressively with the concentration. This point is interesting to note as it confirms that the slight dilution variations in the various hydrolysis ratio in Figure 1A are not important enough to transform 100% DW nanotubes into 100% SW nanotubes.

From the SAXS curves, it is possible to extract the proportion of SW and DW nanotubes using a mixture of both SW and DW form factors. The results of such an analysis correspond to the lines in Figure 3. The obtained proportions are given in Table 1.

Figure 4 shows the cryo-TEM images obtained of the same samples. In the cryo-TEM images, DW and SW nanotubes are clearly distinguished simultaneously. Therefore, we have used the cryo-TEM images to assess the SW/DW proportions. Table 1 contains the proportions that have been obtained for all aluminum initial concentrations using the SAXS curves or the cryo-TEM images.

Table 1. Proportions of SW and DW Nanotubes as a Function of the Initial Aluminum Concentration Determined by SAXS and Using Cryo-TEM Images

C_{al} (M)	proportions "cryo-TEM"	proportions "SAXS"
0.25	100% DW	100% DW
0.4	100% DW	100% DW
0.5	80% DW/20% SW	75% DW/25% SW
0.6	53% DW/47% SW	60% DW/40% SW
0.75	28% DW/72% SW	25% DW/75% SW

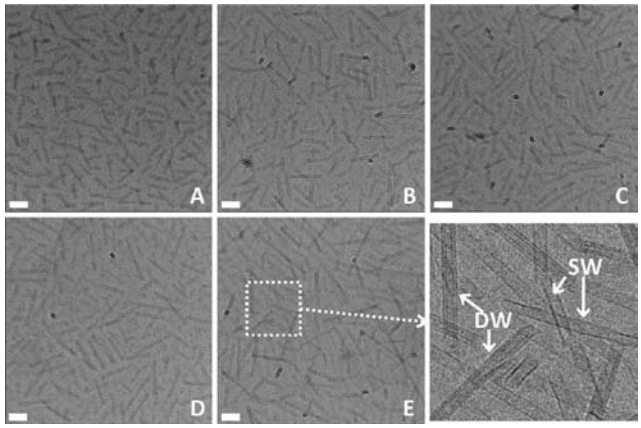

Figure 4. Cryo-TEM images of samples prepared with an initial aluminum concentration of (A) 0.25 M, (B) 0.4 M, (C) 0.5 M, (D) 0.6 M, and (E) 0.75 M (scale bar is 20 nm). A zoom in the case of image E illustrates the mixture of SW and DW nanotubes in the same sample.

Of course, the previously described control through a modification of the hydrolysis ratio at an initial concentration of 0.5 M of aluminum perchlorate also applies for the other concentrations. For example, at 0.25 M and R = 2, the SAXS curve is showing a 100% DW signal. If the hydrolysis ratio is lowered to R = 1.75, then SW nanotubes are obtained. For the 0.75 M sample at R = 2, a majority of SW nanotubes is observed by SAXS. However, increasing the hydrolysis ratio to R = 2.5 produces DW nanotubes.

SW and DW Nanotubes Have the Same Local Structure. On these samples, we have measured the X-ray adsorption spectra at the Ge K edge. The obtained spectra are displayed in Figure 5. Beside differences due to the important noise level at large k values, all spectra in Figure 5 exhibit almost the same shape. Partial EXAFS curves were fitted using back-Fourier transforms with filters in the 1−3.6 Å range.

Table 2 presents the best fits for all samples. Results are extremely similar, and only one fit is shown in Figure 5 as an example.

For all samples, the Ge atomic local scale determined by EXAFS is that of imogolite for which Ge is surrounded by 4 oxygen atoms in the first coordination sphere (Ge tetrahedron) and linked to 6 Al octahedra with Ge−Al distance of 3.23 ± 0.02 Å.

We have observed that both the initial reactant concentration and the hydrolysis ratio OH/Al enable a control over the final imogolite-like nanotube structure. In the case of the concentration variation, this transition from DW to SW occurs

dx.doi.org/10.1021/ja209756j | J. Am. Chem. Soc. 2012, 134, 3780−3786

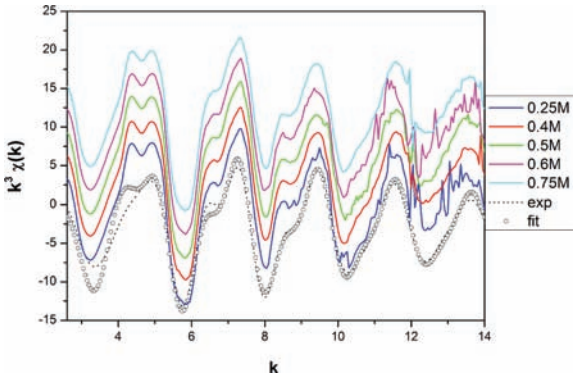

Figure 5. $k^3\chi(k)$ spectra for the samples obtained at 0.25, 0.4, 0.5, 0.6, and 0.75 M of initial aluminum perchlorate concentration. Partial experimental curve (back-Fourier transform from 1 to 3.6 Å) of the 0.5 M sample as compared to the fitted curve.

Table 2. EXAFS Parameters of the Calculated Spectra[a]

	Ge−O first coordination sphere			Ge−Al secoond coordination sphere		
conc (M)	N_{Ge-O}	R_{Ge-O}	σ_{Ge-O}	N_{Ge-Al}	R_{Ge-Al}	σ_{Ge-Al}
0.25	4	1.75	0.034	6	3.22	0.070
0.4	4	1.75	0.045	6	3.24	0.073
0.5	4	1.74	0.043	6	3.25	0.078
0.6	4	1.74	0.021	6	3.23	0.079
0.75	4	1.76	0.049	6	3.25	0.076

[a] N is the coordination number (±10%), R is the radial distance (±0.01 Å), and σ is the Debye−Waller factor (Å).

with the same local structure for the imogolite walls. It is also possible at any tested concentration to go from SW to DW nanotubes by changing the hydrolysis ratio R, with a low hydrolysis ratio being in favor of SW nanotubes and a high hydrolysis ratio leading to DW nanotubes. At a given hydrolysis ratio, the change of the reactant concentration is modifying the SW/DW nanotube proportion as well. The change from one morphology to the other is a progressive transformation rather than a critical transition. We will now propose a model, the objectives of which are: (i) to propose a mechanism for the SW/DW transition, (ii) to explain why triple wall or higher order multi walls do not exist, and (iii) to give possible reason why no DW nanotubes have ever been observed in the case of AlSi imogolite.

Experimental Constraint for the Proposed Model. Our former works tend to demonstrate that the volume fraction of solids does not evolve after the hydrolysis step.[20] This means that the initially formed protoimogolite pieces essentially transform themselves from a roof-tile shape[17] into a tubular shape without significant modifications of the solid volume fraction or structural changes at the local scale. A recent paper[18] confirms by NMR and electrospray ionization mass spectroscopy that a population of protoimogolites is formed in the first 20 h before heating. These protoimogolites transform into nanotubes by condensation and internal rearrangements. These findings suggest that the control over the SW or DW structure lies in this initial transformation. It is reasonable to anticipate that two processes will be of importance.

The first important process is the modification of the protoimogolite curvature required to go from a SW to a DW structure.[11] To describe this part of the process, it is possible to describe protoimogolite as flexible sheets having a natural curvature controlled by the nature (Si or Ge) and amount of adsorbed tetrahedra.

The second process of importance is the attractive interaction between protoimogolites. Gustafson has published results for the zeta potential of single-walled AlSi imogolites.[27] He found a point of zero charge (PZC) at pH of 11.5 showing that the imogolite surface properties are dominated by positive charges carried by Al−OH and Al_2−OH external surface sites. More recently, Arancibia-Miranda et al.[28] measured the isoelectric point (IEP) of both protoimogolite and imogolite. They observed a transition form an IEP of about 7 for protoimogolite to 11 at the end of the reaction. This transition is explained by the fact that the exposed surface contains less SiOH surface groups. Indeed, as the protoimogolites transform into imogolites, the SiOH surface groups are no longer directly accessible. This tends to shift the IEP toward higher pH. The initially "bipolar" characteristic of the protoimogolite with one surface dominated by Al_2OH surface sites and the other by SiOH surface sites could give rise to an overall electrostatic attractive potential between them. The observations of the cryo-TEM images before the heating stage where only protoimogolites are formed tend to demonstrate that attractive interactions exist between protoimogolites. Indeed, it is clearly seen that protoimogolite pieces tend to form aggregates. The same association hypothesis has recently been made to interpret DLS results on protoimogolite suspensions.[18]

An Energy-Based Model To Explain SW/DW Transition. To progress in our understanding of the SW/DW transition, we propose a simple model. We will first describe it qualitatively and then give some quantitative insights.

Let us consider protoimogolites as flexible thin sheets of matter having a spontaneous curvature with a positive surface charge on one side and a negative charge on the other. Two protoimogolite pieces attract each other at least because of the electrostatic attraction between the positive charge of the external wall of the first sheet and negative charge of the internal wall of the second sheet and because of van der Waals interactions and interprotoimogolite hydrogen-bond network. The flexibility of these two sheets allows increasing or decreasing their curvature at the expense of elastic energy. When strongly attached protoimogolite pieces transform into a DW imogolite, one of the piece increases its curvature as compared to the spontaneous curvature and the other reduces it. These two transformations yield an overall increase in elastic energy ΔE_c. In such a simple scenario, two outcomes are possible as depicted in Figure 6. In the first one, at the end of

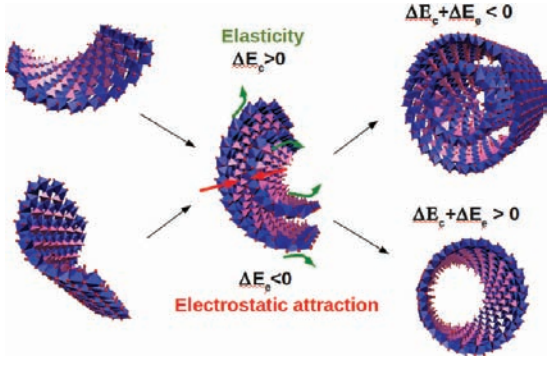

Figure 6. Qualitative schematic scenario for the protoimogolite transformation into SW or DW imogolite nanotubes.

dx.doi.org/10.1021/ja209756j | J. Am. Chem. Soc. 2012, 134, 3780−3786

the curvature modifications, the loss of attractive energy ΔE_e is more than the gain of elastic energy ΔE_c ($\Delta E_e + \Delta E_c < 0$), and a DW nanotube is obtained. In the second one, at the end of the curvature modifications, the loss of electrostatic energy is less than the gain in curvature energy ($\Delta E_e + \Delta E_c > 0$). Thus, the two curved pieces cannot sustain the transformation; the protoimogolites detach, and SW nanotubes are obtained. This type of free energy balance between attractive interaction energy and internal curvature energy could also theoretically result in the production of multi wall nanotubes.

Still at the qualitative level, the interesting question is now to understand the effect of reactants concentrations and hydrolysis ratio modifications on these two scenarios. In the case of the reactant concentration variations, the ionic strength is modified. The change of ionic strength controls the amplitude of the electrostatic attractive energy between protoimogolites. At high reactant concentrations (i.e., high ionic strength), the strength of the protoimogolite stacking is reduced, and they will not sustain the curvature energy gain needed to curve while being coupled. Thus, SW nanotubes are prevailing at high reactants concentrations. At low reactant concentrations, on the contrary, the electrostatic screening is lowered, and the strength of protoimogolite stacking is higher. The protoimogolites can then sustain the increased curvature energy.

When the hydrolysis ratio is lowered, a transition toward SW is also observed, whereas the ionic strength is only slightly decreased. Thus, this type of transition does not come from a screening effect. It has been demonstrated[29] that upon reduction of the hydrolysis ratio, defects and lacuna appear in the imogolite wall. This has two consequences. First, it increases the proportion of AlOH surface sites. This modifies the amount of surface charge as a function of pH as the pK_a of Al_2OH and AlOH surface sites are different.[27] The loss of electrostatic attraction or hydrogen-bond energy weakens the protoimogolite stacking and leads to SW structure as observed when the hydrolysis ratio is lowered. The occurrence of lacuna in the dioctahedral layer can also modify the mechanical properties of the imogolite. This modification is however not trivial as not only Al lacuna occur but also Si lacuna. The prevailing effects could be either an increase or a decrease of the natural curvature. To our knowledge, up to now, no theoretical investigation of the impact of lacuna on the mechanical properties of imogolites was published.

From a quantitative point of view, Konduri et al. and Guimareas et al. have explored the total internal energy of single wall aluminosilicate nanotubes.[10] The effect of Si substitution by Ge atoms on this energy as a function of the imogolite curvature has also been studied.[11] In their model, the energy is essentially linked to the stretching or compression of Al−O, Si−O, and Ge−O bonds around their equilibrium values. Comparing this simple strain energy model to molecular dynamic calculations, Konduri et al. give equilibrium bond lengths and harmonic force constants for the Al−O, Si−O, and Ge−O bonds, respectively.

It is possible to propose a continuum model where the imogolite is considered as a thick solid with different surface tension contributions on both sides. The mechanical energy due to curvature modification can thus be approximated by:[10b]

$$E(R) = E_0 + Yh^3/R^2 + \Delta\sigma h/R \quad (1)$$

where $2h$ is the thickness of the imogolite wall, Y is the Young modulus, and $\Delta\sigma$ is the difference in surface tension between the outer and inner surfaces. With such model, the natural curvature of the nanotube is $1/R_c = -\Delta\sigma/2Yh^2$. Figure 7 displays the values obtained by Konduri and the curves corresponding to an adjustment of E_0, Y, and $\Delta\sigma$ with this simple model.

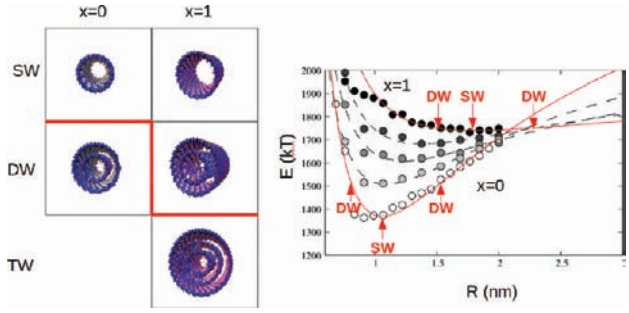

Figure 7. Left: Molecular models for AlGe ($x = 1$) and AlSi ($x = 0$) SW, DW, and AlGe TW imogolites. Above the red lines, the structures have been experimentally observed. Right: Total internal energy for $Al(Ge_xSi_{(1-x)})$ containing an average of 200 Al atoms according to Konduri et al.[11] The lines correspond to adjustment of eq 1.[10b]

Assuming the same variation for the elastic energy of the external and internal wall and a separation of 2 Å between the two walls, the total elastic energy variation for a SW/DW transformation of nanotubes containing on average 200 Al atoms is ∼20, 50, 84, 161, and 280 kT for, respectively, $x = 1$, 0.75, 0.5, 0.25, and 0 in $Al(Ge_xSi_{(1-x)})$ nanotubes. It is also possible to predict the curvature energy variation for a triple wall AlGe nanotube, and we find ∼80 kT. It is worth noting that there is probably some extra coupling between the internal and external walls of DW AlGe imogolite. Indeed, the internal gap corresponds to the size of a water molecule. The gap could contain water and charge compensating ions. This would create specific interactions between the walls that were not taken into account in the Konduri model. These couplings are therefore not accounted for in this simple approach.

The second term concerns the attractive energy variation upon curvature modification as depicted in Figure 6. We have no experimental information about the adhesion energy between imogolite walls. We can assume a maximum adhesion energy of 33 mJ/m^2 equivalent to mica sheets adhesion in water.[30] A protoimogolite containing 200 Al atoms has an average surface of about 15 nm^2, which yields a maximum sustainable elastic energy variation of 120 kT. With such a maximum adhesion energy, SW/DW transition would be possible down to $x = 0.5$ in $Al(Ge_xSi_{(1-x)})$ nanotubes, and TW AlGe imogolites would form. As no TW form, most probably the adhesion energy between the protoimogolites is below 22 mJ/m^2. The existence of DW imogolite below $x = 1$ may not be in contradiction with the experimental results of Konduri et al.[10a] that show that the experimental radius of $Al(Ge_xSi_{(1-x)})$ nanotubes does not change very much for $x > 0.5$. Further refinement of the quantitative model could be proposed using calculations of the electrostatic interaction between concentric tubes. From the experimental point of view, the measurements of the SW to DW transitions for mixture of Si and Ge atoms would be of the highest interest.

■ CONCLUSION

Our experiments clearly show that protoimogolites exist very early in the synthesis process (already at $R = 0.5$). These

dx.doi.org/10.1021/ja209756j | J. Am. Chem. Soc. 2012, 134, 3780−3786

protoimogolites have been now identified by several independent investigations as being a mixture of curved pieces with imogolite-like structure. Cryo-TEM observations in the present work clearly show the presence of aggregates, thus demonstrating attractive interactions between the inner and outer surface of the protoimogolite structure. DLS results have also been interpreted through the assumption of protoimogolite attractive interactions.[18] The protoimogolite aggregates transform progressively into single-walled or double-walled nanotubes. None of the explored conditions allow the formation of triple-walled or other multiwalled nanotubes. We show that the SW and DW have the same wall structure, but their curvature difference induces shifts in some IR bands (743 cm^{-1} for SW to 695 cm^{-1} for DW). It is a very important observation, which gives the possibility for one to distinguish the two structures with a widespread and easily used experimental technique.

We propose a model where the preferential final structure is decided by the balance between the attractive energy that tends to maintain the tube in close contact and the curvature energy that is accumulated during this transformation. This mechanism is to our knowledge the only example of a physicochemical control of an inorganic nanotube curvature and morphology with an almost atomic precision in diameter. Thus, a high yield of perfectly defined nanotubes is obtained without the need of complex post-treatments as is required, for example, in the case of carbon nanotubes.

■ ASSOCIATED CONTENT

Supporting Information

Procedure for the calculation of electronic density profiles and scattering form factors. This material is available free of charge via the Internet at http://pubs.acs.org.

■ AUTHOR INFORMATION

Corresponding Author

antoine.thill@cea.fr

Notes

The authors declare no competing financial interest.

■ ACKNOWLEDGMENTS

We thank Nicolas Menguy and Eric Larquet for the impressive cryo-TEM work. We thank the SWING Beamline of the synchrotron Soleil where part of the SAXS experiments was performed. This work has been partially supported by the iCEINT GDR (www.i-ceint.org) and the IMOtox ANSES program. Cnano Ile de France is also acknowledged for his support for the IR spectrometer.

■ REFERENCES

(1) Yoshinaga, N.; Aomine, A. *Soil Sci. Plant Nutr. (Richmond, Aust.)* **1962**, *8*, 22−29.

(2) Cradwick, P. D. G.; Farmer, V. C.; Russell, J. D.; Masson, C. R.; Wada, K.; Yoshinaga, N. *Nature (London), Phys. Sci.* **1972**, *240*, 187−189.

(3) Wada, K.; Yoshinaga, N. *Am. Mineral.* **1969**, *54*, 50−71.

(4) Barron, P. F.; Wilson, M. A.; Campbell, A. S.; Frost, R. L. *Nature* **1982**, *299*, 616−618.

(5) MacKenzie, K. J. D.; Bowden, M. E.; Brown, I. W. M.; Meinhold, R. H. *Clays Clay Miner.* **1989**, *37*, 317−324.

(6) Farmer, V. C.; Fraser, A. R.; Tait, J. M. *Geochim. Cosmochim. Acta* **1979**, *43*, 1417−1420.

(7) Bursill, L. A.; Peng, J. L.; Bourgeois, L. N. *Philos. Mag. A* **2000**, *80*, 105−117.

(8) Wada, S. I.; Wada, K. *Clays Clay Miner.* **1982**, *30*, 123−128.

(9) Farmer, V. C.; Fraser, A. R.; Tait, J. M. *J. Chem. Soc., Chem. Commun.* **1977**, 462−463.

(10) (a) Konduri, S.; Mukherjee, S.; Nair, S. *Phys. Rev. B: Condens. Matter Mater. Phys.* **2006**, *74*, 033401. (b) Guimaraes, L.; Enyashin, A. N.; Frenzel, J.; Heine, T.; Duarte, H. A.; Gotthard, S. *ACS Nano* **2007**, *1*, 362−368.

(11) Konduri, S.; Mukherjee, S.; Nair, S. *ACS Nano* **2007**, *1*, 393−402.

(12) Demichelis, R.; Noel, Y.; D'Arco, P.; Maschio, L.; Orlando, R.; Dovesi, R. *J. Mater. Chem.* **2010**, *20*, 10417−10425.

(13) Lee, S. U.; Choi, Y. C.; Youm, S. G.; Sohn, D. *J. Phys. Chem. C* **2011**, *115*, 5226−5231.

(14) Creton, B.; Bougeard, D.; Smirnov, K. S.; Guilment, J.; Poncelet, O. *J. Phys. Chem. C* **2008**, *112*, 10013−10020.

(15) Levard, C; Rose, J.; Masion, A.; Doelsch, E.; Borschneck, D.; Olivi, L.; Dominici, C.; Grauby, O.; Woicik, J. C.; Bottero, J. Y. *J. Am. Chem. Soc.* **2008**, *130*, 5862−5863.

(16) Mukherjee, S.; Kim, K.; Nair, S. *J. Am. Chem. Soc.* **2007**, *129*, 6820−6826.

(17) Levard, C.; Rose, J.; Thill, A.; Masion, A.; Doelsch, E.; Maillet, P.; Spalla, O.; Olivi, L.; Cognigni, A.; Ziarelli, F.; Bottero, J. Y. *Chem. Mater.* **2010**, *22*, 2466−2473.

(18) Yucelen, G. I.; Choudhury, R. P.; Vyalikh, A.; Scheler, U.; Beckham, H. W.; Nair, S. *J. Am. Chem. Soc.* **2011**, *133*, 5397−5412.

(19) Maillet, P.; Levard, C.; Larquet, E.; Mariet, C.; Spalla, O.; Menguy, N.; Masion, A.; Doelsch, E.; Rose, J.; Thill, A. *J. Am. Chem. Soc.* **2010**, *132*, 1208−1209.

(20) Maillet, P.; Levard, C.; Spalla, O.; Masion, A.; Rose, J.; Thill, A. *Phys. Chem. Chem. Phys.* **2011**, *13*, 2682−2691.

(21) Lindner, P. *Neutrons, X-rays and Light: Scattering Methods Applied to Soft Condensed Matter*; North-Holland: Amsterdam, 2002.

(22) Michalowicz, A. *Logiciels pour la Chimie*; Société Française de Chimie: Paris, 1991; pp 102−103.

(23) Michalowicz, A. *J. Phys. IV* **1997**, *IV*, 235.

(24) Ankudinov, A. L.; Ravel, B.; Rehr, J. J.; Conradson, S. D. *Phys. Rev. B: Condens. Matter Mater. Phys.* **1998**, *58*, 7565−7576.

(25) Martin, F.; Ildefonse, P.; Hazemann, J. L.; Petit, S.; Grauby, O.; Decarreau, A. *Eur. J. Mineral.* **1996**, *8*, 289−299.

(26) Bac, B. H.; Song, Y.; Kim, M. H.; Lee, Y. B.; Kang, I. M. *Chem. Commun.* **2009**, 5740−5742.

(27) Gustafsson, J. P. *Clays Clay Miner.* **2001**, *49*, 73−79.

(28) Arancibia-Miranda, N.; Escuey, M.; Molina, M.; Garcia-Gonzalez, M. T. *J. Non-Cryst. Solids* **2011**, *357*, 1750−1756.

(29) Levard, C.; Masion, A.; Rose, J.; Doelsch, E.; Borschneck, D.; Olivi, L.; Chaurand, P.; Dominici, C.; Ziarelli, F.; Thill, A.; Maillet, P.; Bottero, J. Y. *Phys. Chem. Chem. Phys.* **2011**, *13*, 14516−14522.

(30) Shubin, E.; Kekicheff, P. *J. Colloid Interface Sci.* **1993**, *155*, 108−123.